Nucleon-hyperon interaction from Lattice QCD near the physical point

Takahiro M. Doi[1,*] and Noriyoshi Ishii[1,†]

[1] *Research Center for Nuclear Physics (RCNP), Osaka University, 567-0047, Japan*

I. INTRODUCTION

Interactions between hadrons are important for understanding the origin of matter. Although most matter is composed of nucleons, which are composed of u,d quarks, hyperons, which are baryons containing strange quarks, are thought to appear in the interiors of high-density objects such as neutron stars. Therefore, the study of the interaction between nucleons and hyperons is an important theme to understand properties of neutron stars.

In this report, the Lattice QCD study on the interaction between a nucleon(N) and a hyperon containing a single strange quark (strangeness= -1), namely, the Λ baryon and the Σ baryon, is shown. Specifically, coupled-channel $\mathrm{N}\Lambda - \mathrm{N}\Sigma$ potentials are considered in the case of the total isospin $I = 1/2$, and a single channel $\mathrm{N}\Sigma$ potential is considered in the case of the total isospin $I = 3/2$. For each of them, only the central potential is considered in the case of the total spin $S = 0$ and the central potential and tensor potential are considered in the case of the total spin $S = 1$.

Since the nucleon is the lightest baryon, and Λ and Σ baryons are the next lightest baryons after the nucleon, they are important hadrons in nuclear and hadron physics. This lightness of mass results in a poor signal-to-noise ratio in numerical calculations, and it is difficult to calculate the potentials with sufficient accuracy[1]. In this report, we would like to discuss an improved partial-wave decomposition on a lattice to obtain results with better accuracy than before. At the same time, we discuss the problems that need to be solved in the future, which have become clear as a result of the improved accuracy of the calculations.

This report is organized as follows. In Sec. 2, a method for calculating hadron interactions from the lattice QCD, the HAL QCD method [2–6] is explained. In Sec. 3, a method for performing partial wave expansion on a lattice, the Misner's method[8, 9] is explained. In Sec. 4, nucleon-hyperon potentials obtained from actual lattice QCD calculations are shown. Section 5 is devoted to the summary of this report.

II. HAL QCD METHOD

In this section, we will describe a method for calculating hadron-hadron interactions using the lattice QCD, called the HAL QCD method [2–6].

First, we briefly explain the lattice QCD [10–12]. Baryons are composite particles of quarks and gluons, and there are strong interactions between quarks and gluons. Although the fundamental theory of the strong interaction is known to be Quantum chromodynamics(QCD), the quantitative study is quite difficult with analytical calculations based on perturbation theory due to the nature of strong coupling in the low energy region (asymptotic freedom). The lattice QCD is QCD formulated on a lattice, and physical quantities are calculated non-perturbatively by quantum Monte Carlo methods. First-principle calculations by the lattice QCD can explain the masses of almost ground state hadrons [13, 14], and this is currently the most reliable non-perturbative method for investigating properties of hadrons.

Next, we will explain HAL QCD method, which is a way to obtain hadron-hadron interactions using lattice QCD [2–6]. Here we show the case of interaction between two baryons. In the HAL QCD method, the scattering process of two hadrons on a lattice is considered and a quantity that reproduces the scattering phase shift is constructed, called Nambu-Bethe-Salpeter(NBS) wave function

$$\psi(\boldsymbol{r}) = \langle 0|B(\boldsymbol{r},t)B(\boldsymbol{0},t)|B(k)B(-k);W\rangle, \qquad (1)$$

where $B(\boldsymbol{r},t)$ is a local interpolating sink operator for a baryon and $|B(k)B(-k);W\rangle$ is the source state with total energy W of two baryons. At long distance $|\boldsymbol{r}| \equiv r > R$, where R is the interaction range, the NBS wave function satisfies the Helmholtz equation

$$(\nabla^2 + k^2)\psi(\boldsymbol{r}) = 0, \qquad (2)$$

then the phase shift of scattering of two hadrons can be obtained from this equation. Here, the NBS wave function can be regarded as a relative wave function of the two hadrons. Then, the inter-baryon potential can be constructed to reproduce the NBS wave function as the solution of the Schrodinger equation

$$(\nabla^2 + k^2)\psi(\boldsymbol{r}) = m\int d\boldsymbol{r}' U(\boldsymbol{r},\boldsymbol{r}')\psi(\boldsymbol{r}') \qquad (3)$$

inside of the interaction range $r < R$. U is the HAL QCD potential between the two hadrons.

Some characteristics of the scattering phase shift and hadron-hadron potential energy obtained by the HAL QCD method are described below. First, the scattering phase shift is a physical quantity that can be compared to the scattering phase shift obtained in actual experiments. While the potential energy itself is not a physical

*takahiro.doi@rcnp.osaka-u.ac.jp
†ishiin@rcnp.osaka-u.ac.jp

quantity, at least it guarantees that it reproduces the scattering phase shift. Although the above potential energy is non-local, a local potential can be obtained by the velocity expansion

$$U(\boldsymbol{r},\boldsymbol{r}') = V_{\rm C}(r) + V_{\rm T}(r)S_{12} + V_{\rm LS}(r)\boldsymbol{L}\cdot\boldsymbol{S} + \cdots, \quad (4)$$

where the first term is the central force of the leading order, the second term is the tensor force of the leading order, the third term is the LS force of the next to the leading order. These local potentials can be easily applied to many-body calculations.

In the actual calculation, the 4-point correlator of baryons

$$G_{BB}(\boldsymbol{r},t) = \langle 0|B(\boldsymbol{r},t)B(\boldsymbol{0},t)|\overline{J_{\rm src}(t=0)}|0\rangle, \quad (5)$$

is calculated. $J_{\rm src}(t=0)$ is a source operator of two baryons and the overline denotes complex conjugate. If the time interval t between the source and sink operators is sufficiently large and the ground state saturation is satisfied, this 4-point correlator gives the NBS wave function (1). However, if a sufficiently large t is taken, the signal-to-noise ratio becomes exponentially small. Thus it is impractical to take the large-t limit.

The time-dependent HAL QCD method solves this problem [7]. In the time-dependent HAL QCD method, we consider the quantity

$$R(\boldsymbol{r},t) \equiv G_{BB}(\boldsymbol{r},t)/{\rm e}^{-2mt}, \quad (6)$$

where m is the mass of the Baryon B. For general t that is not large enough, it includes the contribution of excited states as well as ground states

$$R(\boldsymbol{r},t) = \sum_i A_{W_i}\psi_{W_i}(\boldsymbol{r}){\rm e}^{-(W_i-2m)t}, \quad (7)$$

where i is the label of the energy eigenstates and W_i is the total energy. We note that below the elastic threshold, all the excited states share the same potential energy U as

$$(\nabla^2 + k_{W_i}^2)\psi_{W_i}(\boldsymbol{r}) = m\int d\boldsymbol{r}' U(\boldsymbol{r},\boldsymbol{r}')\psi_{W_i}(\boldsymbol{r}'). \quad (8)$$

In fact, all of these equations can be combined into a single equation

$$(-\frac{\partial}{\partial t} + \frac{1}{4m}\frac{\partial^2}{\partial t^2} + \frac{\nabla^2}{m})R(\boldsymbol{r},t) = \int d\boldsymbol{r}' U(\boldsymbol{r},\boldsymbol{r}')R(\boldsymbol{r}',t). \quad (9)$$

This equation itself can be derived without the expression of the expansion (7), and means that all the excited states below the elastic threshold gives the signal in the calculation of the potential U. In other words, there is no need to take the large-t limit for the ground state saturation. This method highly improves the accuracy of the calculation, and then the HAL QCD method is currently the most reliable for the calculation of hadron-hadron interactions.

Since the nucleon-hyperon potential in the case of strangeness$=-1$ is considered in this study, we need to consider the coupled channels of $\mathrm{N\Lambda}-\mathrm{N\Sigma}$ and S-wave and D-wave [1, 4–6]. For example, the coupled-channel potentials in the case of the total isospin and spin $(I,S)=(1/2,1)$ are obtained as

$$V_{\rm I=1/2,S=1} = \Psi^{-1}K, \quad (10)$$

$$V_{\rm I=1/2,S=1} = \begin{pmatrix} V_{\rm C}^{\mathrm{N\Lambda-N\Lambda}} & V_{\rm T}^{\mathrm{N\Lambda-N\Lambda}} & V_{\rm C}^{\mathrm{N\Lambda-N\Sigma}}\Delta_{\mathrm{N\Sigma}}^{\mathrm{N\Lambda}} & V_{\rm T}^{\mathrm{N\Lambda-N\Sigma}}\Delta_{\mathrm{N\Sigma}}^{\mathrm{N\Lambda}} \\ V_{\rm C}^{\mathrm{N\Sigma-N\Lambda}}\Delta_{\mathrm{N\Lambda}}^{\mathrm{N\Sigma}} & V_{\rm T}^{\mathrm{N\Sigma-N\Lambda}}\Delta_{\mathrm{N\Lambda}}^{\mathrm{N\Sigma}} & V_{\rm C}^{\mathrm{N\Sigma-N\Sigma}} & V_{\rm T}^{\mathrm{N\Sigma-N\Sigma}} \end{pmatrix}, \quad (11)$$

$$\Psi = \begin{pmatrix} R_{\rm S}^{\mathrm{N\Lambda-N\Lambda}} & R_{\rm D}^{\mathrm{N\Lambda-N\Lambda}} & R_{\rm S}^{\mathrm{N\Lambda-N\Sigma}} & R_{\rm D}^{\mathrm{N\Lambda-N\Sigma}} \\ 2\sqrt{2}R_{\rm D}^{\mathrm{N\Lambda-N\Lambda}} & 2\sqrt{2}R_{\rm S}^{\mathrm{N\Lambda-N\Lambda}} - 2R_{\rm D}^{\mathrm{N\Lambda-N\Lambda}} & 2\sqrt{2}R_{\rm D}^{\mathrm{N\Lambda-N\Sigma}} & 2\sqrt{2}R_{\rm S}^{\mathrm{N\Lambda-N\Sigma}} - 2R_{\rm D}^{\mathrm{N\Lambda-N\Sigma}} \\ R_{\rm S}^{\mathrm{N\Sigma-N\Lambda}} & R_{\rm D}^{\mathrm{N\Sigma-N\Lambda}} & R_{\rm S}^{\mathrm{N\Sigma-N\Sigma}} & R_{\rm D}^{\mathrm{N\Sigma-N\Sigma}} \\ 2\sqrt{2}R_{\rm D}^{\mathrm{N\Sigma-N\Lambda}} & 2\sqrt{2}R_{\rm S}^{\mathrm{N\Sigma-N\Lambda}} - 2R_{\rm D}^{\mathrm{N\Sigma-N\Lambda}} & 2\sqrt{2}R_{\rm D}^{\mathrm{N\Sigma-N\Sigma}} & 2\sqrt{2}R_{\rm S}^{\mathrm{N\Sigma-N\Sigma}} - 2R_{\rm D}^{\mathrm{N\Sigma-N\Sigma}} \end{pmatrix}, \quad (12)$$

$$K = {\rm diag}\left(k(\mathrm{N\Lambda}), k(\mathrm{N\Lambda}), k(\mathrm{N\Sigma}), k(\mathrm{N\Sigma})\right)\Psi, \quad (13)$$

where some parameters are defined as

$$k({\rm NB}) = \frac{1+3\delta_{NB}^2}{8\mu_{NB}}\partial t^2 - \frac{\partial}{\partial t} + \frac{\nabla^2}{2\mu_{\rm NB}}, \quad (14)$$

$$\mu_{\rm NB} \equiv m_{\rm N}m_{\rm B}/(m_{\rm N}+m_{\rm B}), \quad (15)$$

$$\delta_{\rm NB} \equiv (m_{\rm N}-m_{\rm B})/(m_{\rm N}+m_{\rm B}), \quad (16)$$

$$\Delta_{\rm NB_2}^{\rm NB_1} \equiv \exp[-(m_{\rm B_2}-m_{\rm B_1})]. \quad (17)$$

Here, $V_{\rm C}$ is the central potential and $V_{\rm T}$ is the tensor potential, and there are diagonal and off-diagonal components because of the coupled channel. We consider the 2×2 coupled-channel equation in the case of $(I,S)=(1/2,0),(3/2,1)$ and the single-channel equation

in the case of $(I,S)=(3/2,0)$. Moreover, $R_{\rm S}$ and $R_{\rm D}$ are correlators (6) of S-wave and D-wave, respectively, defined by the partial wave decomposition.

However, the partial wave expansion on a lattice is nontrivial because a box lattice does not have the continuous rotation symmetry. A possible way to obtain an approximate S-wave is to use the A_1^+ projection on the cubic group [3, 15]

$$R_S(\boldsymbol{r}) = R^{A_1^+}(\boldsymbol{r}) \equiv \frac{1}{48}\sum_{g\in O_h} R(g^{-1}\boldsymbol{r}), \tag{18}$$

and the D-wave can be obtained as $R_{\rm D}(\boldsymbol{r}) = R(\boldsymbol{r}) - R_S(\boldsymbol{r})$. In this method, there is contribution as noises from the high orbital angular momentum ($L=4,6,\cdots$). A clever method of partial wave expansion on a lattice has been proposed, called Misner's method [8] in this report, and it has been applied to the HAL QCD potential of $\mathrm{N\Lambda_c}$ system[9]. In this study, we apply it to the partial wave decomposition of correlators in the coupled-channel system.

III. MISNER'S METHOD

In this section, we explain the partial wave expansion on the lattice.

The partial wave decomposition is the expansion of a function $\psi(\boldsymbol{r}) = \psi(r,\theta,\phi)$ in a three dimensional space in terms of the spherical harmonics $Y_{lm}(\theta,\phi)$ as

$$\psi(r,\theta,\phi) = \sum_{l=0}^{\infty}\sum_{m=-l}^{l} g_{lm}(r) Y_{lm}(\theta,\phi). \tag{19}$$

In the continuum case, we can obtain $g_{lm}(r)$ by taking the spherical surface integral at fixed r as

$$g_{lm}(r) = \int_S d\Omega \overline{Y_{lm}(\theta,\phi)}\psi(r,\theta,\phi) \tag{20}$$

thanks to the orthonormal property of Y_{lm}. This holds even in a finite box.

However, in the discrete space, $g_{lm}(r)$ is difficult to obtain by the formula (20) because the number of points with distance r is finite. Misner's method is a clever way to obtain $g_{lm}(r)$ even on a lattice.

First, the Misner's method in continuum space is explained. In addition to the angular directions, the basis functions in the radial direction are introduced as

$$G_n^{R,\Delta}(r) = \frac{1}{r}\sqrt{\frac{2n+1}{2\Delta}} P_n\left(\frac{r-R}{\Delta}\right), \tag{21}$$

where $P_n(r)$ is the Legendre polynomial, and they are orthonormal in the radial interval $[R-\Delta, R+\Delta]$. Then, a new orthonormal basis function $\mathcal{Y}_{nlm}^{R,\Delta}(r,\theta,\phi) \equiv G_n^{R,\Delta}(r)Y_{lm}(\theta,\phi)$ is defined and this satisfies the orthonormal relation in a spherical shell $S_{R,\Delta} \equiv \{\boldsymbol{r}|R-\Delta \le r \le R+\Delta\}$ as

$$\int_{S_{R,\Delta}} d^3x \overline{\mathcal{Y}_{nlm}^{R,\Delta}(r,\theta,\phi)}\mathcal{Y}_{n'l'm'}^{R,\Delta}(r,\theta,\phi) = \delta_{nn'}\delta_{ll'}\delta_{mm'}. \tag{22}$$

Thus the new decomposition of $\psi(r,\theta,\phi)$ is defined as

$$\psi(r,\theta,\phi) = \sum_{n=0}^{\infty}\sum_{l=0}^{\infty}\sum_{m=-l}^{l} c_{nlm}^{R,\Delta}\mathcal{Y}_{nlm}^{R,\Delta}(r,\theta,\phi) \tag{23}$$

with the coefficients $c_{nlm}^{R,\Delta}$, which is calculated by

$$c_{nlm}^{R,\Delta} = \int_{S_{R,\Delta}} d^3x \overline{\mathcal{Y}_{nlm}^{R,\Delta}(r,\theta,\phi)}\psi(r,\theta,\phi). \tag{24}$$

The desired amplitude $g_{lm}(r)$ for $R-\Delta \le r \le R+\Delta$ can be calculated as

$$g_{lm}(r) = \sum_{n=0}^{\infty} c_{nlm}^{R,\Delta} G_n^{R,\Delta}(r). \tag{25}$$

In the discrete space, the volume integral is replaced by the discrete sum as

$$\int_{S_{R,\Delta}} d^3x \to \sum_{\boldsymbol{x}} \omega^{R,\Delta}(\boldsymbol{x}), \tag{26}$$

where $\boldsymbol{x}$ denotes a site vector on a lattice, and $\omega^{R,\Delta}(\boldsymbol{x})$ is a weight factor corresponding to a volume of the overlapped region between the shell $S_{R,\Delta}$ and a unit cube around the site $\boldsymbol{x}$. In the previous works [8, 9], the approximate form of $\omega^{R,\Delta}(\boldsymbol{x})$ is taken as $\omega^{R,\Delta}(\boldsymbol{x}) = a^3$ or 0 when a unit cube is inside/outside of the shell and $\omega^{R,\Delta}(\boldsymbol{x}) = a^2(\Delta + a/2 - |R-r|)$ in other case, where a is the lattice spacing. Using the weight factor, an inner product of functions $f(\boldsymbol{x})$ and $g(\boldsymbol{x})$ in the shell $S_{R,\Delta}$ is defined as

$$\langle f|g\rangle_{S_R,\Delta} \equiv \sum_{\boldsymbol{x}} \omega^{R,\Delta}(\boldsymbol{x})\overline{f(\boldsymbol{x})}g(\boldsymbol{x}). \tag{27}$$

Since the orthogonality for $\mathcal{Y}_{nlm}^{R,\Delta}$ is broken on a lattice, the dual basis functions $\tilde{\mathcal{Y}}_{nlm}^{R,\Delta}$ are defined as

$$\tilde{\mathcal{Y}}_{nlm}^{R,\Delta}(\boldsymbol{x}) \equiv \sum_{n=0}^{n_{\max}}\sum_{l=0}^{l_{\max}}\sum_{m=-l}^{l} \mathcal{Y}_{n'l'm'}^{R,\Delta}(\boldsymbol{x})\mathcal{G}^{-1}_{(n'l'm')(nlm)}, \tag{28}$$

where the parameters of upper bounds $n_{\max}$ and $l_{\max}$, and the matirx $\mathcal{G}_{(nlm)(n'l'm')} \equiv \langle \mathcal{Y}_{nlm}^{R,\Delta}|\mathcal{Y}_{n'l'm'}^{R,\Delta}\rangle_{S_R,\Delta}$ are introduced, and it satisfies the orthogonal relation $\langle\tilde{\mathcal{Y}}_{nlm}^{R,\Delta}|\mathcal{Y}_{n'l'm'}^{R,\Delta}\rangle_{S_R,\Delta} = \delta_{nn'}\delta_{ll'}\delta_{mm'}$.

Therefore, decomposition (23) of $\psi(r,\theta,\phi)$ can be approximately performed on a lattice as

$$\psi(r,\theta,\phi) \simeq \sum_{n=0}^{n_{\max}}\sum_{l=0}^{l_{\max}}\sum_{m=-l}^{l} c_{nlm}^{R,\Delta}\mathcal{Y}_{nlm}^{R,\Delta}(r,\theta,\phi) \tag{29}$$

with the coefficient $c^{R,\Delta}_{nlm} = \langle \tilde{\mathcal{Y}}^{R,\Delta}_{nlm} | \psi \rangle_{S_R,\Delta}$. Finally, the desired amplitude $g_{lm}(R)$ can be approximately obtained as

$$g_{lm}(R) \simeq \sum_{n=0}^{n_{\max}} c^{R,\Delta}_{nlm} G^{R,\Delta}_{n}(R). \tag{30}$$

In the actual calculation, we take parameters $n_{\max} = 2$, $l_{\max} = 4$ and $\Delta = a$, which are confirmed to give accurate results of S-wave and D-wave of correlators $R(\boldsymbol{r})$ in the previous study[9].

IV. NUMERICAL RESULTS

In this section, we show the numerical results of $N\Lambda - N\Sigma$ potentials. The Lattice QCD simulations are performed on the gauge configurations in the large volume ($(L/a)^4 = 96^4$) with the lattice spacing a, generated in the (2+1)-flavor lattice QCD with the Iwasaki gauge action at $\beta = 1.82$ and the non-perturbatively O(a)-improved Wilson quark action, together with the stout smearing, at nearly physical quark masses [16] corresponding to $m_\pi \simeq 146$ MeV and $m_K \simeq 525$ MeV. The lattice cutoff is $a^{-1} = 2.333(18)$ GeV ($a = 0.0846(7)$ fm), then the lattice size in physical unit is $L \simeq 8.1$ fm.

After averaging 4 rotations and 96 sources location due to the hypercubic symmetry, we have 414 gauge configurations. We use the jackknife method with bin size 18 to evaluate the statistical errors.

A. $(I, S) = (1/2, 0)$, $N\Lambda - N\Sigma$ central potential

When $(I, S) = (1/2, 0)$, we have to consider $N\Lambda - N\Sigma$ coupled channel. The numerical results of central potentials using A_1^+ projection (18) without Misner's method are shown in Fig.1, and results using Misner's method are shown in Fig.2. We see from the figures that Misner's method makes the error bar small while the change of the central values is small. It is easily seen that $N\Lambda - N\Lambda$ potential at long distance reach to 0 at any t, and some potentials, in particular $N\Sigma - N\Sigma$ potentials at long distance do not reach 0 at any t. This is caused by the contamination of the excited states above the elastic threshold.

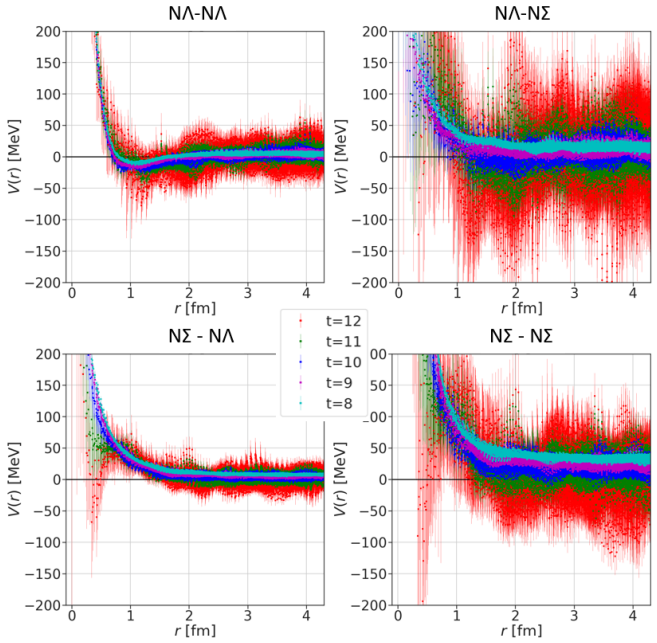

FIG. 1: $N\Lambda - N\Sigma$ coupled-channel central potentials with $I = 1/2$, $s = 0$ and several time intervals t in $[8, 12]$ calculated without Misner's method.

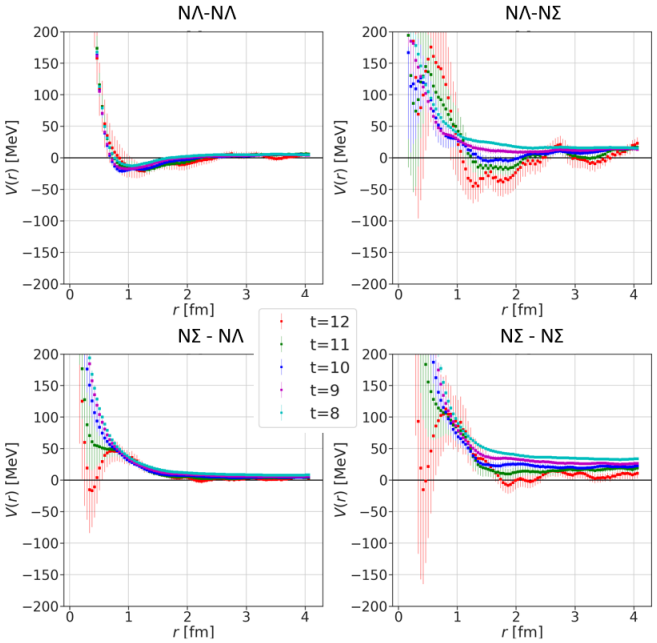

FIG. 2: $N\Lambda - N\Sigma$ coupled-channel central potentials with $I = 1/2$, $s = 0$ and several time intervals t in $[8, 12]$ calculated using Misner's method.

One of the reasons of the contamination of inelastic excited states is understood by study of baryon interactions in the case of flavor SU(3) limit [17]. When $I = 1/2$ and $S = 0$ in the case SU(3) limit, $N\Lambda$ and $N\Lambda$ states

are represented by the flavor basis as

$$\begin{pmatrix} \langle \mathrm{N\Lambda}| \\ \langle \mathrm{N\Sigma}| \end{pmatrix} = \begin{pmatrix} \sqrt{\frac{9}{10}} & -\sqrt{\frac{1}{10}} \\ \sqrt{\frac{1}{10}} & \sqrt{\frac{9}{10}} \end{pmatrix} \begin{pmatrix} \langle \mathbf{27}| \\ \langle \mathbf{8}_s| \end{pmatrix}. \tag{31}$$

From the previous study [17], the potential in the state $\langle \mathbf{27}|$ is attractive, and the potential in the state $\langle \mathbf{8}_s|$ is repulsive. In general, the repulsive channel includes more excited states than the attractive channel. Since the $N\Sigma$ state is almost the repulsive state $\langle \mathbf{8}_s|$, we can understand why the $N\Sigma$ potential suffers from the inelastic excited states. Moreover, some potentials with large t show wavy behavior.

Due to the contamination of the inelastic excited states and the wavy behavior, at least the $N\Sigma$ central potential is not reliable in the case of $I = 1/2$ and $S = 0$. Then, we expect the other method to reduce the contribution of the undesirable inelastic excited states. Although the wall source and the point sink operators are utilized for calculation of the correlators in this study, there is still room for improvement of better source and sink operators.

B. $(I, S) = (1/2, 1)$, $N\Lambda - N\Sigma$ central and tensor potentials

When $(I, S) = (1/2, 1)$, we have to consider the $N\Lambda - N\Sigma$ coupled channel, and there are central and tensor potentials. The numerical results of central and tensor potentials using Misner's method are shown in Fig.3 and Fig.4, respectively. Unlike the case of $(I, S) = (1/2, 0)$, all the potentials reach 0 at long distance and stable for t. Thus the potentials in this case are reliable.

These good signals are also understood by SU(3) limit study. When $I = 1/2$ and $S = 0$ in the case SU(3) limit, $N\Lambda$ and $N\Lambda$ states are represented by the flavor basis as

$$\begin{pmatrix} \langle \mathrm{N\Lambda}| \\ \langle \mathrm{N\Sigma}| \end{pmatrix} = \begin{pmatrix} \sqrt{\frac{1}{2}} & -\sqrt{\frac{1}{2}} \\ \sqrt{\frac{1}{2}} & \sqrt{\frac{1}{2}} \end{pmatrix} \begin{pmatrix} \langle \mathbf{10}^*| \\ \langle \mathbf{8}_a| \end{pmatrix}. \tag{32}$$

From the previous study [17], the potentials in the states $\langle \mathbf{10}^*|$ and $\langle \mathbf{8}_a|$ are attractive. Thus we can understand that the contamination of the inelastic excited states is small and the signals of the potentials are good in this case.

C. $(I, S) = (3/2, 0)$, $N\Sigma$ central potential

When $(I, S) = (3/2, 0)$, there is only the $N\Sigma$ central potential. The numerical results of central potentials using Misner's method are shown in Fig.5. The potentials reach to 0 at long distance and stable for t. Thus the potential in this case is reliable.

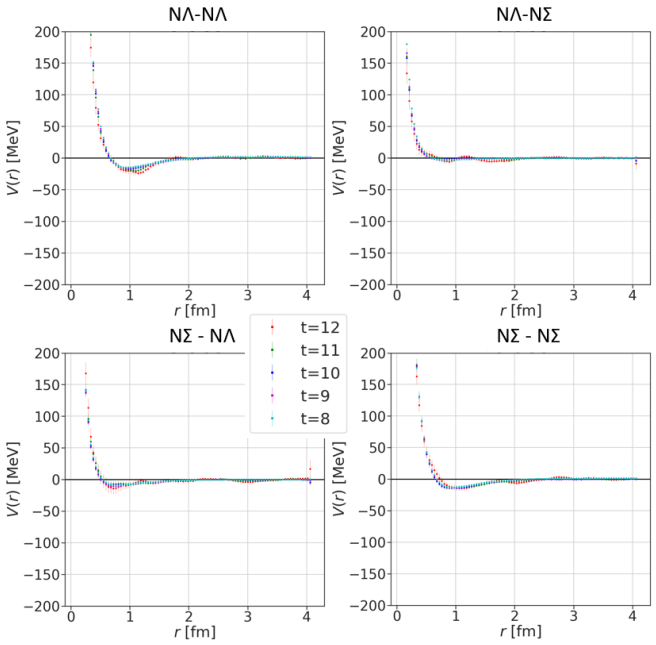

FIG. 3: $N\Lambda - N\Sigma$ coupled-channel central potentials with $I = 1/2$, $s = 1$ and several time intervals t in $[8, 12]$ calculated by Misner's method.

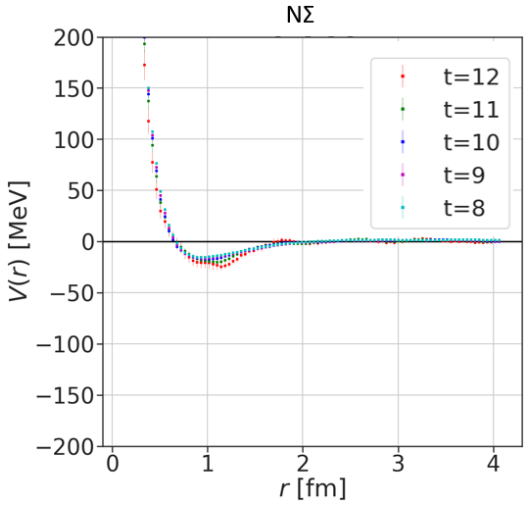

FIG. 5: $N\Sigma$ central potentials with $I = 3/2$, $s = 0$ and several time intervals t in $[8, 12]$ calculated using Misner's method.

The good signal in this case is also consistent with the SU(3) limit study, where the potential for the channel $\langle \mathrm{N\Sigma}| = \langle \mathbf{27}|$ is attractive.

D. $(I, S) = (3/2, 1)$, $N\Sigma$ central and tensor potentials

When $(I, S) = (3/2, 1)$, there are the $N\Sigma$ central and tensor potentials. The numerical results of central and tensor potentials using Misner's method are shown in Fig.6. Although the tensor potential reaches 0 at the

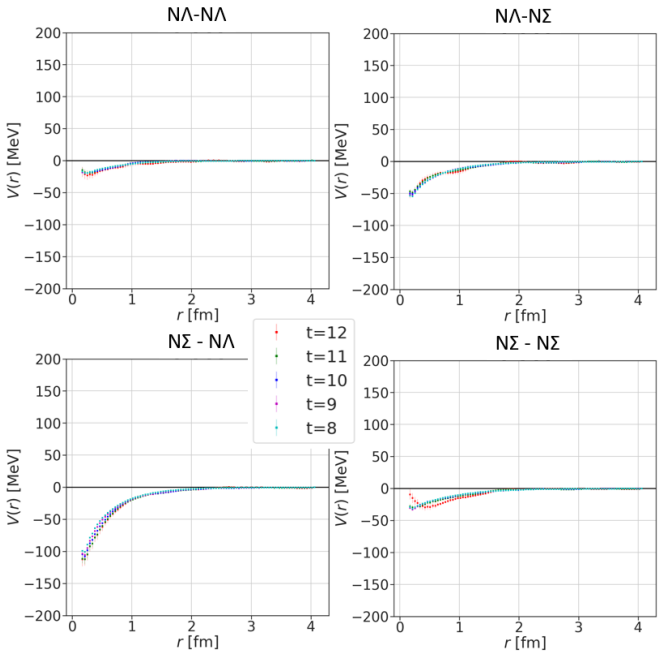

FIG. 4: $N\Lambda - N\Sigma$ coupled-channel tensor potentials with $I = 1/2$, $s = 1$ and several time intervals t in $[8, 12]$ calculated using Misner's method.

long distance, the central potential does not reach 0 at the long distance with any t. Like the case of $I = 1/2$ and $S = 0$, those potential suffer from the inelastic excited states.

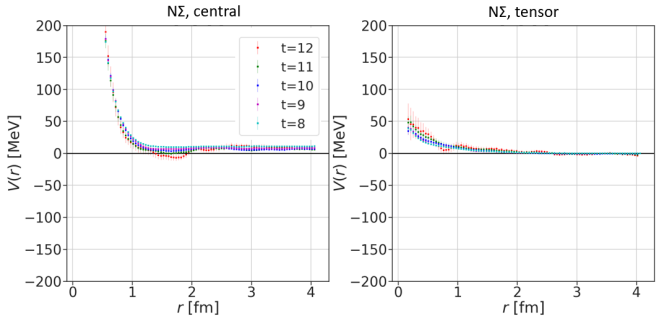

FIG. 6: $N\Sigma$ central(left) and tensor(right) potentials with $I = 3/2$, $s = 1$ and several time intervals t in $[8, 12]$ calculated using Misner's method.

In fact, this state corresponds to the 10-plet state, which is Pauli almost forbidden, as $\langle N\Sigma| = \langle \mathbf{10}|$, where the corresponding potential is strongly repulsive. Then, the bad signal is understood.

V. SUMMARY

In this report, we show the baryon-baryon potentials in the channel with strangeness= -1 obtained by the first-principle calculation of the lattice QCD. The method for the calculation of the hadron-hadron interaction, HAL QCD method, and the method for the partial wave decomposition on a lattice, Misner's method, are briefly explained. Thank to the Misner's method, the noises from the high orbital angular momentum ($L = 4, 6, \cdots$) are reduced, then the statistical errors of the baryon-baryon potentials becomes small. However, the accurate results make us notice that some potentials are found not to reach 0 at long distances and to show wavy behavior, and the results suffer from the problem of the contamination of the inelastic excited states in the case of $(I, S) = (1/2, 0), (3/2, 1)$. The reason for the problem is that $\langle N\Sigma|$ state corresponds to a repulsive channel in the flavor basis, and includes many excited states. This behavior is understood by the previous SU(3) limit study of the baryon-baryon interaction [17].

In the future, other methods to reduce the contribution of the inelastic excited states will be developed, and more reliable potentials between nucleon-hyperon will be calculated at the physical point, which means physical quark masses. Then the potentials can be applied to many-body calculations of nucleons and hyperons and lead to the elucidation of the inner structure of neutron stars, solution of the hyperon puzzle, and so on.

Acknowledgments

The lattice QCD calculations have been performed on the K computer at RIKEN (hp120281, hp130023, hp140209, hp150223, hp150262, hp160211, hp170230), HOKUSAI FX100 computer at RIKEN (G15023, G16030, G17002) and HA-PACS at University of Tsukuba(14a-20, 15a-30). We thank ILDG/JLDG [18–20] which serves as an essential infrastructure in this study. This work is supported in part by the Grant-in-Aid of the Japanese Ministry of Education, Sciences and Technology, Sports and Culture (MEXT) for Scientific Research (Nos.JP16H03978, JP18H05236, JP18H05407, JP19K03879), by SPIRE (Strategic Program for Innovative REsearch), by Priority Issue on Post-K computer (Elucidation of the Fundamental Laws and Evolution of the Universe) and by Joint Institute for Computational Fundamental Science (JICFuS).

[1] H. Nemura et al., EPJ Web Conf. **175**, 05030 (2018).
[2] N. Ishii, S. Aoki, and T. Hatsuda, Phys. Rev. Lett. **99**, 022001 (2007).
[3] S. Aoki, T. Hatsuda, and N. Ishii, Prog. Theor. Phys. **123**, 89 (2010).
[4] S. Aoki et al. [HAL QCD Collaboration], Proc. Japan

Acad. B **87**, 509 (2011).
[5] S. Aoki, B. Charron, T. Doi, T. Hatsuda, T. Inoue and N. Ishii, Phys. Rev. D **87** (2013) 034512.
[6] K. Sasaki et al. [HAL QCD Collaboration], PTEP **2015**, 113B01 (2015).
[7] N. Ishii et al. [HAL QCD Collaboration], Phys. Lett. B **712**, 437 (2012).
[8] C. W. Misner, Class. Quant. Grav. **21**, S243 (2004).
[9] T. Miyamoto et al., Phys. Rev. D **101**, 074514 (2020).
[10] K. G. Wilson, Phys. Rev. D **10**, 2445 (1974).
[11] M. Creutz, *Quarks, Gluons and Lattices*, Cambridge University Press, Cambridge, England (1985).
[12] H. J. Rothe, *Lattice Gauge Theories*, World Scientific, Singapore (2012).
[13] S. Durr et al. [BMW collaboration], Science **322**, 1224 (2008).
[14] Sz. Borsanyi et al., Science **347**, 1452 (2015).
[15] M. Lüscher, Nucl. Phys. B **354**, 531 (1991).
[16] K.-I. Ishikawa et al. [PACS Collaboration], PoS LATTICE **2015**, 075 (2016).
[17] T. Inoue et al. [HAL QCD Collaboration], Prog. Theor. Phys. **124**, 591 (2010).
[18] International Lattice Data Grid (ILDG), (Available at:http://plone.jldg.org/).
[19] Japan Lattice Data Grid (JLDG), (Available at:http://www.jldg.org/).
[20] T. Amagasa, et al., J. Phys. Conf. Ser. **664**, 042058 (2015).